



HAL
open science

Antibacterial and Photocatalytic Properties of ZnO Nanostructure Decorated Coatings

Souad Abou Zeid, Anne Perez, Stéphane Bastide, Marie Le Pivert, Stéphanie Rossano, Hynd Remita, Nicolas Hautière, Yamin Leprince-Wang

► **To cite this version:**

Souad Abou Zeid, Anne Perez, Stéphane Bastide, Marie Le Pivert, Stéphanie Rossano, et al.. Antibacterial and Photocatalytic Properties of ZnO Nanostructure Decorated Coatings. *Coatings*, 2023, 14 (1), pp.41. 10.3390/coatings14010041 . hal-04447912

HAL Id: hal-04447912

<https://hal.science/hal-04447912>





Submitted on 18 Apr 2024

HAL is a multi-disciplinary open access archive for the deposit and dissemination of scientific research documents, whether they are published or not. The documents may come from teaching and research institutions in France or abroad, or from public or private research centers.

L'archive ouverte pluridisciplinaire **HAL**, est destinée au dépôt et à la diffusion de documents scientifiques de niveau recherche, publiés ou non, émanant des établissements d'enseignement et de recherche français ou étrangers, des laboratoires publics ou privés.

Article

Antibacterial and Photocatalytic Properties of ZnO Nanostructure Decorated Coatings

Souad Abou Zeid ¹, Anne Perez ², Stéphane Bastide ³, Marie Le Pivert ⁴, Stéphanie Rossano ², Hynd Remita ⁴, Nicolas Hautière ⁵ and Yamin Leprince-Wang ^{1,*}

¹ ESYCOM, CNRS-UMR9007, Université Gustave Eiffel, F-77454 Marne-la-Vallée, France; souadabouzeid321@gmail.com

² LGE, Université Gustave Eiffel, F-77454 Marne-la-Vallée, France; anne.perez@univ-eiffel.fr (A.P.); stephanie.rossano@univ-eiffel.fr (S.R.)

³ ICMPE, CNRS-UMR 7182, Université Paris-Est Créteil (UPEC), F-94320 Thiais, France; stephane.bastide@cnrs.fr

⁴ ICP, CNRS-UMR 8000, Université Paris-Saclay, F-91405 Orsay, France; marie.le-pivert@universite-paris-saclay.fr (M.L.P.); hynd.remita@universite-paris-saclay.fr (H.R.)

⁵ COSYS-IMSE, Université Gustave Eiffel, F-77454 Marne-la-Vallée, France; nicolas.hautiere@univ-eiffel.fr

* Correspondence: yamin.leprince@univ-eiffel.fr

Abstract: Given the growing concern over antibiotic resistance, there is an urgent need to explore alternative antibacterial strategies. Metal oxide nanostructures have emerged as a promising option, and in particular, zinc oxide (ZnO) nanostructures have demonstrated strong antifungal and antibacterial properties. This study focuses on ZnO nanowires (ZnO NWs) and their potential as antibacterial agents against *Pseudomonas putida*, a Gram-negative bacterium. The objective is to investigate the antibacterial mechanisms and assess their efficiency. The unique shape of ZnO NWs, obtained through hydrothermal growth, may rupture bacterial cells and inhibit bacterial growth. In addition to their morphology, the release of Zn²⁺ ions from ZnO NWs may contribute to their antibacterial properties. These ions have the potential to disrupt the bacterial cell membrane, further impeding bacterial growth. Moreover, ZnO nanostructures exhibit excellent photocatalytic properties under UV light, enhancing their antibacterial effects. Overall, this study highlights the potential of hydrothermally synthesized ZnO NWs in inhibiting *P. putida* growth and provides valuable insights into their antibacterial mechanisms. The findings suggest that ZnO nanostructures have the potential to be effective antibacterial agents and could be utilized in various settings to fight microbial infections and maintain hygiene.

Keywords: ZnO nanowires (ZnO NWs); hydrothermal growth synthesis; antibacterial activity; photocatalysis; surface modification; coating



Citation: Abou Zeid, S.; Perez, A.; Bastide, S.; Le Pivert, M.; Rossano, S.; Remita, H.; Hautière, N.; Leprince-Wang, Y. Antibacterial and Photocatalytic Properties of ZnO Nanostructure Decorated Coatings. *Coatings* **2024**, *14*, 41. <https://doi.org/10.3390/coatings14010041>

Academic Editor: Joaquim Carneiro

Received: 22 November 2023

Revised: 17 December 2023

Accepted: 24 December 2023

Published: 27 December 2023



Copyright: © 2023 by the authors. Licensee MDPI, Basel, Switzerland. This article is an open access article distributed under the terms and conditions of the Creative Commons Attribution (CC BY) license (<https://creativecommons.org/licenses/by/4.0/>).

1. Introduction

Bacterial biofilm formation, which refers to the colonization of surfaces by pathogenic microbes, is a significant concern in healthcare and industrial settings. This issue is particularly problematic for surfaces that require sterilization, such as medical implants, hospital surfaces, and various medical devices. The severity of this problem is compounded by the growing prevalence of resistance to antibiotics among microbial species, leading to a notable surge in postoperative infections and associated fatalities in recent times [1–4]. In a glimpse into the future, economic projections paint a distressing picture; if we fail to forge new paths in antibacterial therapies, bacterial infections could be responsible for upward of 10 million deaths per annum by 2050 (Figure 1) [5].

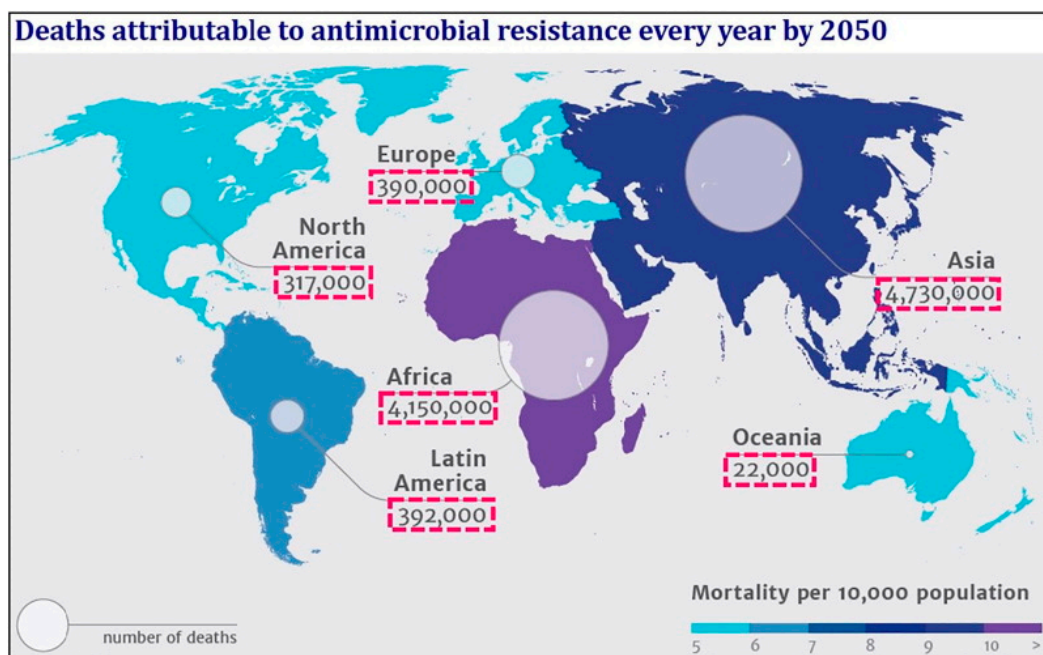


Figure 1. Geographical representation of the projected 10 million deaths by 2050 attributable to antimicrobial resistance worldwide. (Source: The Review on Antimicrobial Resistance—Tackling drug resistant infections globally, 2014) [5].

To address this concern, extensive research has been devoted to the development of surfaces with specific antibacterial properties, in order to curb the formation of bacterial biofilms. Two primary strategies have emerged as viable means to mitigate the formation of bacterial biofilms. The first approach involves incorporating antimicrobial or inhibitory agents, such as metal nanoparticles [6–9], antibiotics [10], and polymer compounds [11,12], onto the outer surface of biocompatible materials. This strategy relies on the chemical activity of these agents to inhibit biofilm formation. Alternatively, the second approach focuses on the micro/nanostructuring of surfaces in order to induce mechanical perturbation, which will induce rupture of cell membranes upon contact with these nanostructures, thus exerting a physical “kill” activity. Together, these strategies showcase a multidimensional approach to prevent bacterial colonization, encompassing both chemical and physical interventions [13,14]. Pure chemical approaches, as long-term antibacterial solutions, have encountered a decreasing viability primarily due to a rise in resistance to antibiotics [15], concerns regarding the whispered worries of nanomaterial toxicity [16], the tangled enigma of dosage complications [17], and the lack of durability in a biological environment [18,19]. Antibacterial nanostructures that are effective as a result of the physical effects of the surface are widely found in nature. Examples include the native nanopillar arrays on clanger cicada wings (*Psaltoda claripennis* or *P. claripennis*), dragonfly wings (*Diplacodes bipunctata*), and hierarchically structured, self-cleaning lotus leaves [20–22]. These natural surfaces have paved the way for the development of numerous biomimetic, synthetic counterparts [14,18,23–25]. The nanostructures found on *P. claripennis* wings have a diameter of approximately 60 nm, with a height of about 200 nm, and are spaced approximately 170 nm apart (Figure 2a) [20,21]. The attachment of bacteria to the nanostructures initiates a series of mechanical rupturing steps. As the bacteria adhere to the nanostructures, the surface area of their cell membrane significantly increases, particularly in the region suspended between the nanostructures. This stretching of the bacterial cell membranes eventually reaches a critical point, causing membrane breaking and rendering the bacteria inactive [20,21,26]. It has been reported that this bacterial rupture relies on a mechanical mechanism facilitated by nanostructures, operating independently of surface components [21].

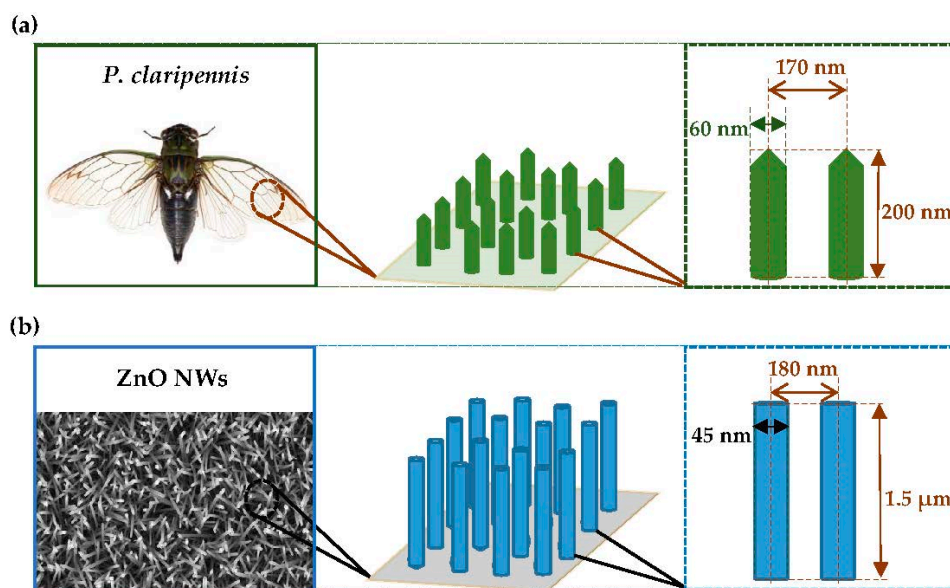


Figure 2. Schematic illustrations of nanostructures (a) on the wing of *P. claripennis* and (b) of ZnO NWs.

As nanostructures inspired by clanger cicada wings, black silicon (bSi) containing high-aspect-ratio nanoprotusions on its surface has been produced using a simple reactive-ion etching (RIE) technique [27]. These nanoprotusions boast a diameter ranging from 20 to 80 nm, a height of 500 nm, and an impressive spacing of 200 to 1800 nm [28]. Upon contact with the bSi surface, bacteria experience mechanical disruption, leading to their rupture. This finding highlights the potential of artificial nanostructures to deliver antibacterial effects that are not reliant on surface components, offering promise for fighting drug-resistant bacteria. However, the creation of a bSi-based antibacterial surface involves the use of top-down nanotechnologies, which are not favored for biomaterial applications. A preferable alternative lies in the fabrication of antibacterial surfaces using bottom-up nanotechnologies. In this regard, the chemical synthesis of (nano)materials is a versatile and powerful means for the development of materials and surfaces with the desired structure, morphology, and chemical composition [29,30].

Among various nanomaterials, ZnO nanostructures have attracted significant attention due to their photocatalytic activity, along with their exceptional biocompatibility, especially when compared to titanium dioxide (TiO_2) [31]. Notably, ZnO nanostructures are also nontoxic in contrast to TiO_2 and other inorganic photocatalytic materials, making them highly desirable for a wide range of applications in both biological and environmental settings [32,33]. ZnO is a II-VI oxide semiconductor with a strong ionic character of chemical bonds [34]. Under ambient conditions, ZnO has a wurtzite crystalline structure with a hexagonal unit cell and two lattice parameters, a and c , with a c/a ratio between 1.5393 and 1.6035 that is transformed into a metastable rock salt structure at high pressures [35]. ZnO is characterized by a direct wide band gap energy (3.37 eV at 300 K), strong adsorption ability, high excitation binding energy (~ 60 meV), high isoelectric point (IEP, ~ 9.5), rapid electron-transfer ability, and high photocatalytic activity, with applications in water and air treatments [36–41]. In addition, ZnO is a low-cost, chemically stable, and amphoteric material. Several methods have been developed for the synthesis of ZnO nanostructures of different morphologies and quality, including vapor–liquid–solid (VLS) growth [36,42], microemulsion synthesis [43], metal organic chemical vapor deposition (MOCVD) [44], and solvothermal [45] and hydrothermal [46,47] methods.

In this study, we focus specifically on ZnO nanowires (ZnO NWs) synthesized via the hydrothermal growth method (Figure 2b), aiming to explore their antibacterial potential against the growth of *Pseudomonas putida* (*P. putida*), a Gram-negative bacteria strain, and shed light on their mechanisms of action. Previous research has primarily focused on the

bactericidal properties of ZnO nanoparticles (ZnO NPs) [48–50], while the potential of ZnO NWs remains relatively unexplored. The distinctive one-dimensional structure of these nanowires offers several advantages, including increased surface accessibility and enhanced photocatalytic activity, which may further increase their antibacterial efficiency.

Several chemical and physical methods have been used for the synthesis of ZnO NWs. In most of the reported methodologies, a bottom-up approach is preferred due to better control the morphological parameters such as aspect ratio, orientation, defects, surface density, and the compositional flexibility of obtaining heterostructures [35]. Hydrothermal growth has emerged as a popular method for synthesizing ZnO NWs due to its simplicity, scalability, and cost-effectiveness. This technique involves the reaction of precursor materials in an aqueous solution at about 90 °C, leading to the controlled growth of ZnO NWs on various substrates on which a ZnO nucleation seed layer is deposited. By carefully tuning the synthesis parameters, such as the reaction temperature, growth time, pH, and precursor concentration, it is possible to achieve high-quality nanowire arrays with desirable properties.

The antibacterial activity of ZnO nanostructures could be attributed to various mechanisms, including the generation of reactive oxygen species (ROS, such as $\bullet\text{OH}$, $\text{O}_2^{\bullet-}$, and H_2O_2) from their photocatalytic activity and the direct physical contact with bacterial cells [51–54]. Through antibacterial tests and characterization techniques, this study aims to demonstrate the enhanced antibacterial activity of these unique nanostructures. The findings will contribute to the growing knowledge about ZnO nanostructures as promising candidates for combating bacterial infections and may open new avenues for research.

2. Materials and Methods

2.1. Materials

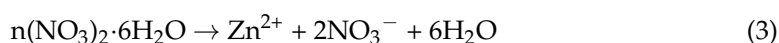
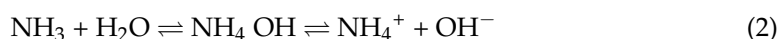
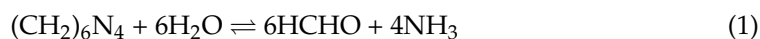
The chemicals and reagents used in the present study and suppliers are given in Table 1. All chemicals were used without further purification. Ultrapure water (Millipore Milli-Q Gradient, 18.2 M Ω cm) was used for all syntheses, and deionized water was used for all rinsing and washing steps. Silicon wafers (*p* type/Boron, <100> \pm 0.5° orientation, resistivity < 0.005 Ω cm) were supplied by Si-Mat (Kaufering, Germany).

Table 1. List of chemicals and reagents used in this study.

Product Name	Chemical Formula/ Composition	Supplier
Zinc acetate dihydrate	$\text{Zn}(\text{CH}_3\text{COO})_2 \cdot 2\text{H}_2\text{O}$	VWR Chemicals, Leuven, Belgium
Poly-vinyl alcohol (PVA)	$(\text{C}_2\text{H}_4\text{O})_x$	Merck KGaA, Darmstadt, Germany
Zinc nitrate hexahydrate	$\text{Zn}(\text{NO}_3)_2 \cdot 6\text{H}_2\text{O}$	CARLO ERBA, Val de Reuil, France
Hexamethylenetetramine (HTMA)	$(\text{CH}_2)_6\text{N}_4$	Merck KGaA, Darmstadt, Germany
Methylthioninium chloride (Methylene Blue hydrate, MB)	$\text{C}_{16}\text{H}_{18}\text{ClN}_3\text{S}$	Sigma Aldrich Chimie S.a.r.l, Saint-Quentin-Fallavier, France
Lysogeny Broth, Miller (LB-Miller)	NaCl, tryptone, and yeast extract	Sigma Aldrich Chimie S.a.r.l, Saint-Quentin-Fallavier, France
Lysogeny Broth with agar, Miller	Agar, NaCl, tryptone, and yeast extract	Sigma Aldrich Chimie S.a.r.l, Saint-Quentin-Fallavier, France
Sodium chloride	NaCl	VWR Chemicals, Leuven, Belgium
Ammonium chloride	NH_4Cl	Thermo Scientific Chemicals, Geel, Belgium
di-sodium hydrogen phosphate anhydrous	Na_2HPO_4	VWR Chemicals, Leuven, Belgium
D-Glucose (dextrose) anhydrous	$\text{C}_6\text{H}_{12}\text{O}_6$	VWR Chemicals, Leuven, Belgium
4-(2 hydroxyethyl)piperazin-1- ylethanesulphonic acid (HEPES)	$\text{C}_8\text{H}_{18}\text{N}_2\text{O}_4\text{S}$	VWR Chemicals, Leuven, Belgium

2.2. Synthesis of ZnO Nanowires

The ZnO NW samples were fabricated using a two-step hydrothermal method on a silicon substrate (Si, 15 mm × 13 mm chip) as described in our previous works [55,56]. Prior to synthesis, the surfaces of Si substrates were thoroughly washed three times for 10 min with ultrapure water using an ultrasonic bath (Elmasonic, Singen, Germany). The substrates were then dried under an air flow and annealed in an oven (Nabertherm, Lilienthal/Bremen, Germany) at 350 °C for 10 min to remove any adsorbed moisture. Subsequently, they were cleaned using a plasma cleaner (Harrick Plasma, Ithaca, NY, USA) to eliminate any adhering particles, as well as organic and inorganic impurities. Once the substrate had undergone a meticulous cleaning ritual, a seed-layer solution, obtained by mixing 10 g of poly-vinyl alcohol (PVA) and 1 g of zinc acetate dihydrate ($\text{Zn}(\text{CH}_3\text{COO})_2 \cdot 2\text{H}_2\text{O}$) in 100 mL of ultrapure water, was spin-coated onto the Si at 3000 rpm for one minute. The resulting thin film was subsequently calcined at 500 °C for 3 h to remove the PVA and facilitate the formation of crystalline ZnO germs on the Si surface. These germs play a crucial role as nucleation centers for promoting the homogeneous growth of ZnO NWs in the subsequent step. For the growth step, a growth solution (25 mM) was prepared by mixing equimolar aqueous solutions of zinc nitrate hexahydrate ($\text{Zn}(\text{NO}_3)_2 \cdot 6\text{H}_2\text{O}$) and hexamethylenetetramine (HMTA, $(\text{CH}_2)_6\text{N}_4$). The solution was preheated to 90 °C in a Teflon-sealed reactor (Servilab, Le Mans, France) prior to introducing the substrate. Subsequently, the ZnO NWs were synthesized on Si at 90 °C for 3 h. During the synthesis, notable reactions took place, as summarized by the following equations (1 to 5). HMTA is a slowly decomposing base that provides an alkaline environment in an aqueous growth solution, and the desired amount of hydroxide ions (OH^-), as shown in Equations (1) and (2), and $\text{Zn}(\text{NO}_3)_2$ supplies the zinc ions (Zn^{2+}), as depicted in Equation (3). These OH^- ions combine with Zn^{2+} ions to form $\text{Zn}(\text{OH})_2$, facilitating the growth of ZnO NWs upon dehydration, as shown in Equations (4) and (5).



Upon completion of the hydrothermal process, the reactors entered a phase of natural cooling. Subsequently, the substrates which recovered the ZnO NWs were carefully extracted and rinsed with ultrapure water to eliminate any lingering reactants or impurities. Afterwards, the samples were dried under an air flow, followed by a postannealing treatment at 350 °C for 30 min to enhance the structural and crystalline qualities of the ZnO NWs.

2.3. Photocatalytic Activity Evaluation

The photocatalytic activity of ZnO NWs was evaluated by the degradation of methylene blue (MB) in an aqueous medium using a UV lamp (Hamamatsu LC-8, Shizuoka, Japan) as an activation source, with a power of 35 mW/cm² (at the sample surface) and a wavelength of 365 nm. At $t = 0$, the ZnO sample was placed in a 30 mL solution of MB, with an initial concentration of 10 μM, and placed under the UV source. The distance between the UV source and the ZnO sample surface was kept at 10 cm during the whole photocatalysis process to ensure the same UV irradiation was received per sample. The aqueous media were continuously stirred throughout the experiments to avoid pollutant mass transfer limitation. The photocatalysis process was monitored by UV-visible spec-

trophotometry (Cary 5000, Agilent Technologies, Les Ulis, France) every 15 min for 3 h. The photodegradation rate (percentage) of MB in the presence or absence of ZnO-NWs was calculated via Equation (6):

$$X(\%) = \left(\frac{A_0 - A_t}{A_0} \right) \times 100 \quad (6)$$

where A_0 is the absorbance value of MB at its maximum absorption wavelength ($\lambda_{\max} = 665$ nm) before irradiation, and A_t is the absorbance value at the same wavelength after a certain time of UV irradiation (t).

2.4. Antibacterial Activity Evaluation: Growth Conditions, Sample Preparation, and Tests

In order to evaluate the antibacterial properties of our ZnO NWs, the ZnO samples were placed in contact with *Pseudomonas putida* (*P. putida*), a Gram-negative bacterium. *P. putida* was grown in a nutritionally rich medium (Lysogeny Broth) and a lighter culture solution (adapted from Valbi et al. [57]). The specific compositions of these media can be found in Table 2. To ensure sterility, the culture media were autoclaved at 121 °C for 30 min. A stock culture of *P. putida* strain was stored in 25% glycerol and used to produce all the cultures for this study. The strain was cultured in 200 mL of sterile Lysogeny Broth (LB) medium, a nutritionally rich medium, at 25 °C with constant shaking at 160 rpm.

Table 2. The composition of the culture media used in the experiments.

Culture Medium	Composition	Sample Name
Lysogeny Broth, Miller	NaCl, 10 g L ⁻¹ Tryptone, 10 g L ⁻¹ Yeast extract, 10 g L ⁻¹	M1
Modified culture solution	Glucose, 1 g L ⁻¹ NH ₄ Cl, 1 g L ⁻¹ NaCl, 0.5 g L ⁻¹ Na ₂ HPO ₄ , 6.06 g L ⁻¹ HEPES buffer, 10 mM	M2

The bacterial cultures were prepared following the steps illustrated in Figure 3. A volume of 200 µL of the stock culture was inoculated in 200 mL of the sterile LB medium (M1) at 25 °C with constant shaking at 160 rpm. The bacteria were left to grow for approximately 24 h. Then, a 1 mL aliquot of the *P. putida* culture (M1') was inoculated in 200 mL of the M2 medium, and the culture was placed in the shaker incubator at 25 °C and 160 rpm. After 24 h, the turbidity of the bacterial solution M2' (1 mL of nonfiltered solution) was recorded spectrophotometrically at 600 nm (OD₆₀₀; optical density at 600 nm) using a UV-1800 Shimadzu UV-vis spectrophotometer. To achieve a standardized bacterial inoculum density, the bacterial solution was eventually diluted in sterile M2, in order to achieve an OD₆₀₀ of 0.2. To avoid potential interference during optical measurements caused by the light scattering properties of the solutions, the same liquid medium without microorganisms but with the same concentration of the studied sample was used as a blank control. The OD₆₀₀ of the *P. putida* suspension (M2') was measured and found to be 0.216.

For CFU (colony-forming unit) calculation, the overnight-grown culture of *P. putida* cells (M2') was serially diluted and plated on LB agar plates. The procedure was as follows:

1. Serial Dilution: First, 100 µL of the overnight-grown culture of *P. putida* was diluted in 900 µL of sterile potassium chloride (KCl, 9 g/L) solution, resulting in a 1:10 dilution (referred to as a 10¹ dilution). This dilution process was repeated seven more times, resulting in 10² to 10⁸ dilutions of M2'.
2. Plating on LB agar: 100 µL of each dilution was evenly distributed on LB agar using a sterile spreader, under a laminar flow hood. The Petri dishes were then incubated overnight.

3. Colony Observation: After overnight incubation, the bacterial colonies were macroscopically observed. The number of CFUs was assumed to be equivalent to the number of live cells in suspension [58].
4. CFU/mL Calculation: The colonies were counted and were used to calculate the CFU/mL (x) in the bacterial suspension ($M2'$) with the help of the following equation,

$$x = \frac{\text{Number of colonies on agar plates} \times \text{Dilution factor of bacterial suspension}}{\text{Volume of suspension used}} \quad (7)$$

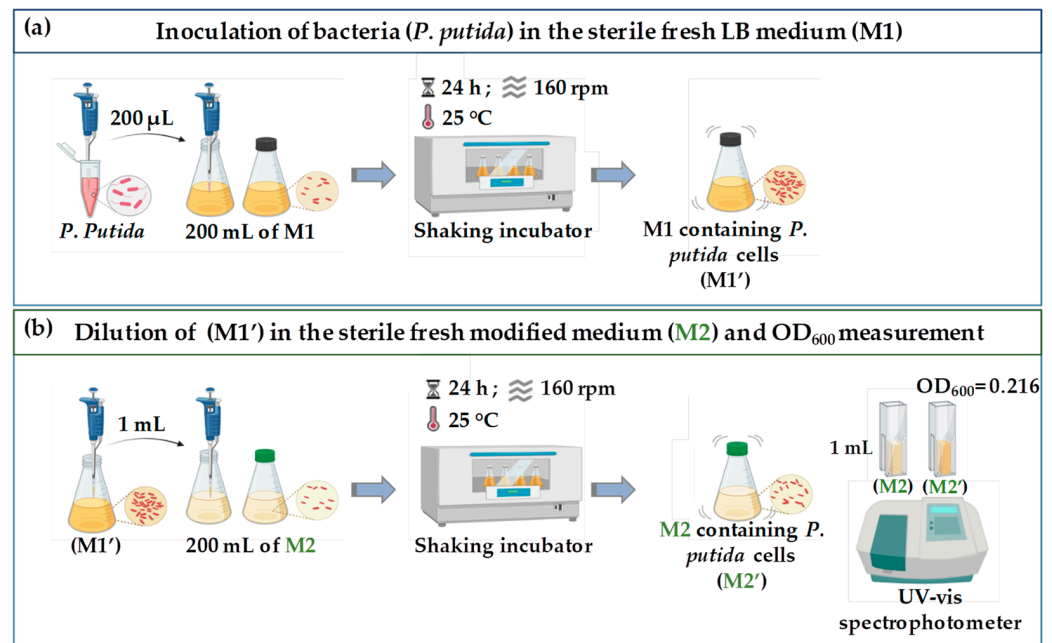


Figure 3. A schematic illustration of the bacterial culture preparation and control. (a) Inoculation of *P. putida* in the sterile fresh LB medium (M1) and (b) Dilution of (M1') in the sterile fresh modified medium (M2) and OD₆₀₀ measurement.

Based on the calculation, the concentration of CFUs in the *P. putida* suspension ($M2'$) was determined to be 4.1×10^7 CFU/mL. This value corresponds to the initial bacterial load in the bacterial solutions, which is used to test the antibacterial efficiency of the ZnO samples.

The antibacterial efficiency of ZnO NWs regarding *P. Putida* was evaluated both with and without UV light exposure. For each experimental condition, two substrates were selected: bare Si, representing the control substrate, and Si/ZnO NWs, representing our prepared sample. The test protocol was as follows:

1. Under a laminar flow hood, both the Si substrate and Si/ZnO NW sample underwent a 30 min UV light disinfection procedure to ensure the surfaces were aseptic.
2. 100 μL of the *P. putida* culture ($M2'$; 4.1×10^7 CFU/mL) was dropped both onto the substrate and sample surfaces.
3. Both substrates were either left in the dark or exposed to UV light at an intensity of 0.17 W/cm^2 for 10 min. This step allowed us to assess the impact of UV light on the antibacterial activity of ZnO NWs and gain an insight into the generation of ROS.
4. The substrates were air-dried for approximately 2 h under the laminar flow hood to allow bacterial adhesion to the surfaces and media evaporation.
5. The inoculated surfaces of the Si and Si/ZnO NWs were gently pressed onto LB agar contained in Petri dishes. This step allowed the transfer of bacterial cells initially deposited on the substrates onto the growth medium.

6. The Petri dishes were placed in an incubator set at 31 °C and allowed to incubate for 24 h, providing optimal conditions for the growth of viable *P. putida* bacterial cells remaining after being in contact with the samples with or without UV light exposure.

In order to investigate the potential release of zinc ions (Zn^{2+}) from ZnO NWs, a series of dissolution experiments was conducted in both the sterile medium M2 and the bacterial culture M2'. The experiments took place in sterile borosilicate Erlenmeyer flasks sealed with cotton plugs, allowing for the free passage of air while maintaining an aerobic aqueous environment. Si/ZnO NW samples were immersed in 100 mL of either M2 or M2', and liquid media were collected at specific time intervals. An amount of 3 mL of each sampled aliquot was filtered using a cellulose acetate filter with a diameter of 0.45 μm , and 1 mL was used for OD_{600} measurements to assess the inhibitory effects of Zn^{2+} on the growth of *P. putida*. The filtered samples were carefully preserved for subsequent analysis using ICP-OES to measure the released concentration of Zn^{2+} .

All antibacterial tests were conducted in triplicates, ensuring the reliability and accuracy of our findings.

2.5. Characterization Techniques

The morphology of the ZnO NWs was investigated by scanning electron microscopy equipped with an InLens detector (FEG-SEM, ZEISS Merlin, Oberkochen, Germany), at an accelerating voltage of 5 kV. To determine the band gap of our ZnO NWs, UV-vis absorption spectra were collected within the wavelength range of 200–800 nm using a UV-vis spectrophotometer (Maya 2000 Pro from Ocean Optics, Duiven, The Netherlands), under a diffuse reflectance configuration. Additionally, UV-vis absorption spectra and the degradation rate of MB were measured using a UV-vis spectrophotometer (Perkin Elmer, Lambda 35, Waltham, MA, USA) in the wavelength range of 300–800 nm. The optical density of *P. Putida* cells in liquid cultures was measured with a UV-1800 Shimadzu UV-vis spectrophotometer. The density of bacterial cells was estimated by determining the optical density at 600 nm (OD_{600}). Additionally, the concentrations of released Zn^{2+} over time were analyzed using inductively coupled plasma optical emission spectrometry (ICP-OES, Perkin Elmer Optima 8300, Waltham, MA, USA).

3. Results

3.1. Unveiling the Morphology and Optical Properties of Prepared ZnO NWs

The surface morphology of the synthesized ZnO NWs supported on the silicon substrate was characterized using SEM. The insert in Figure 4a provides a photographic image of the prepared ZnO NWs. The SEM images in Figure 4a,b displaying top and cross-sectional views of the as-grown ZnO NWs, respectively, show that the nanowires are well vertically aligned, with an average diameter and length of approximately 45 nm and 1.5 μm , respectively, which are consistent with our previous work [55,56,59]. The ZnO NWs' density is around 115 per μm^2 .

A characterization by UV-vis spectrometer measurements in the wavelength range of 300–800 nm was performed at room temperature to characterize the absorbance spectrum and the optical properties of ZnO NWs (Figure 5a). It can be observed that ZnO NWs show a strong absorption in the UV range and quasi-total transparency in the visible range. The high transparency is due to the high optical quality of the sample, testifying for the structural homogeneity and crystallinity of the ZnO-NWs [60]. The band gap is determined with the absorption coefficient and the photon energy ($h\nu$) using the Tauc formula [61,62] (Equation (8)):

$$(\alpha h\nu)^{1/m} = A(h\nu - E_g) \quad (8)$$

where α is the absorption coefficient, $h\nu$ is the photon energy, E_g is the band gap, and $m = 1/2$ for the direct band gap. For the calculation of the band gap, $(\alpha h\nu)^2$ was plotted against the photon energy ($h\nu$), as shown on Figure 5b. The band gap of the prepared ZnO NWs was determined by extrapolating the linear part of the curve down to the $(\alpha h\nu)^2 = 0$

axis. According to the band structure of a semiconductor, the band gap is the difference in energy between the conduction band and the valence band. The reported standard value of the ZnO band gap is 3.37 eV for monocrystalline bulk ZnO [63]. In this investigation, the measured value of the band gap obtained is 3.22 ± 0.01 eV, which is smaller than the bulk ZnO value (3.37 eV) but is similar to the values reported in the literature and in agreement with our previous work. Due to the purity of our material, no significant changes in the band gap values are observed in comparison with the values reported in investigations where ZnO is doped with different metals [64,65] or where modifications are made in the ZnO synthesis parameters (such as pH, growth time, and growth temperature) [41,66–69].

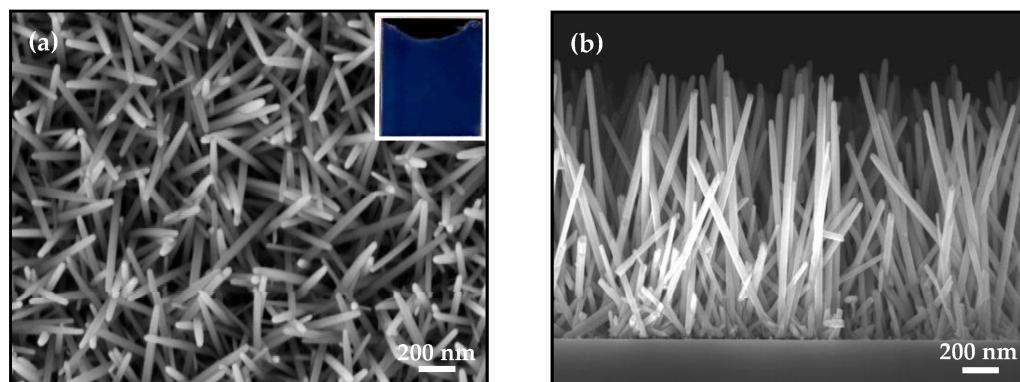


Figure 4. Morphology characterization of the prepared ZnO nanowires grown on a Si substrate at 90 °C for 3 h via a two-step hydrothermal method. (a) Typical SEM image (top view). Inset is a photographic image of the ZnO NWs supported on a silicon substrate (15 mm × 13 mm). (b) Cross-section-view SEM image showing the homogeneous morphology of the ZnO NW array.

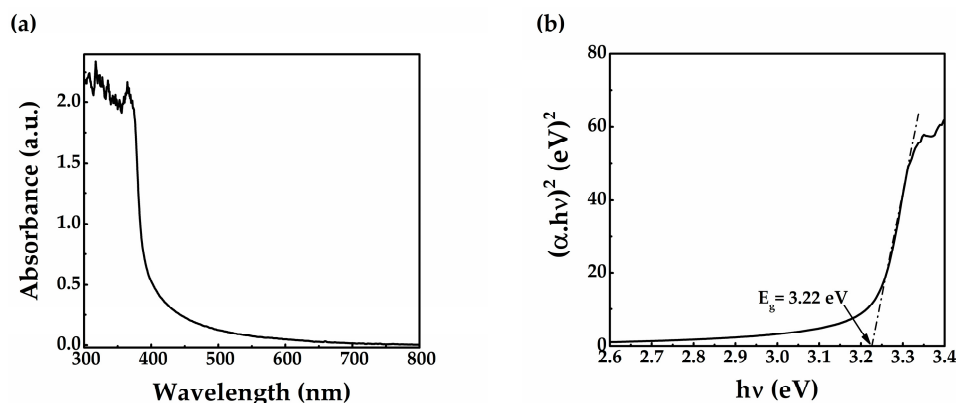


Figure 5. (a) UV-vis absorption spectrum of the ZnO NWs; (b) plots of $(\alpha h\nu)^2$ vs. photon energy for the ZnO NW sample.

3.2. Unveiling the Photocatalytic and Antibacterial Properties of Prepared ZnO Nanowires

ZnO has been considered to be a promising photocatalyst for the degradation of organic contaminant in air and water [70–72]. The photocatalytic activity of the present hydrothermally grown ZnO NWs was evaluated using MB as a model organic pollutant. Figure 6a shows the time-dependent absorption spectra of MB degradation over ZnO nanowires under UV irradiation. It can be seen that the absorbance peak at 665 nm is significantly reduced with increasing irradiation time (Figure 6b), which indicates the degradation of MB molecules. Figure 6c shows the MB photodegradation rate curve as a function of time. A degradation rate of 98% is observed after 120 min, and a degradation rate higher than 99% after 135 min. By comparison, the degradation of MB by UV light only (photolysis) is much slower and less efficient (degradation rate of 40% after 180 min). This demonstrates that ZnO NWs can effectively remove organic pollutants from water, making them a promising method for water purification [52].

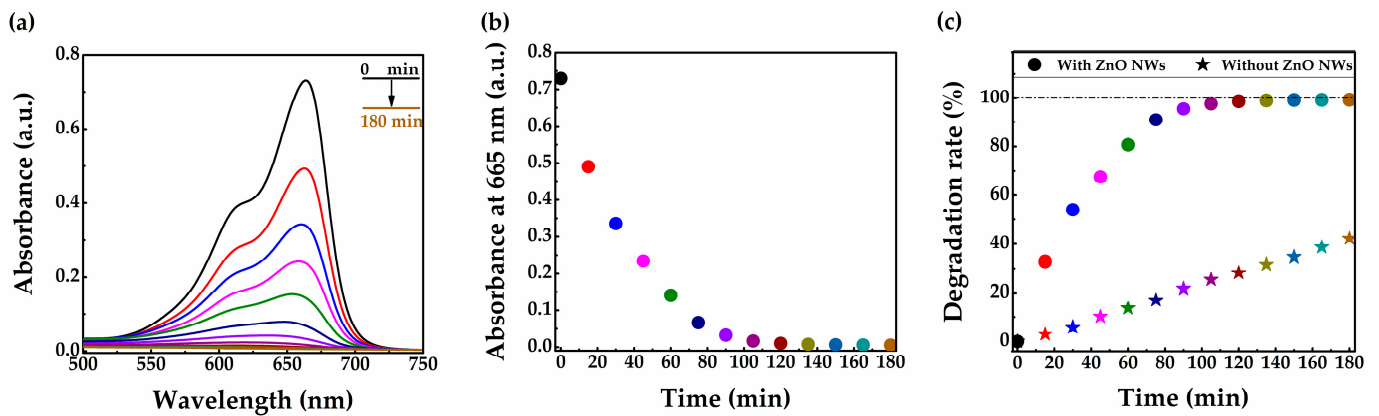


Figure 6. Photocatalytic activity of the ZnO nanowires toward the photodegradation of Methylene Blue (MB): (a) time-dependent UV-vis absorbance spectra of the MB solution using the prepared ZnO NWs as photocatalysts; (b) absorbance at 665 nm vs. time of the MB solution in the presence of the prepared ZnO NWs; and (c) curves of the degradation rate of the MB dye under UV light (~ 365 nm) with (circle) and without (star) ZnO NWs.

The usual antibacterial mechanism of ZnO is related to its photocatalytic properties, particularly the generation of ROS. In this study, our objective was to investigate the antibacterial activity of ZnO NWs under exposure to UV light or in darkness, with the aim of inhibiting bacterial growth. The Petri dishes obtained for both substrates (Si and ZnO NWs) and for the two conditions (in dark (Figure 7a) and under UV light (Figure 7b)) were macroscopically examined for evidence of bacterial growth. Under UV light conditions, no bacterial growth was macroscopically detected around Si/ZnO NWs, in comparison to bare Si which was associated with a pronounced bacterial growth. This evidences that the ZnO NWs coupled with UV light may completely inhibit the growth of *P. Putida*. It seems that the bacteria halo around the bare Si in dark conditions is thicker than the one around the same bare Si under UV light. These results confirm that UV light can be used as a disinfection method but is not efficient enough when not coupled with a photocatalyst. In the absence of UV light, a very thin bacterial halo can be detected around the Si/ZnO NW sample, suggesting that ZnO NWs were less efficient in inhibiting bacterial growth in the absence of UV light. However, a comparison with the bare Si surrounded by a thick halo of bacteria highlights that ZnO NWs alone have a significant impact on preventing the growth of bacteria. The antibacterial activity can be attributed to the ZnO NWs' shape, in terms of diameter and density, which is similar to *P. claripennis* wings [19,20].

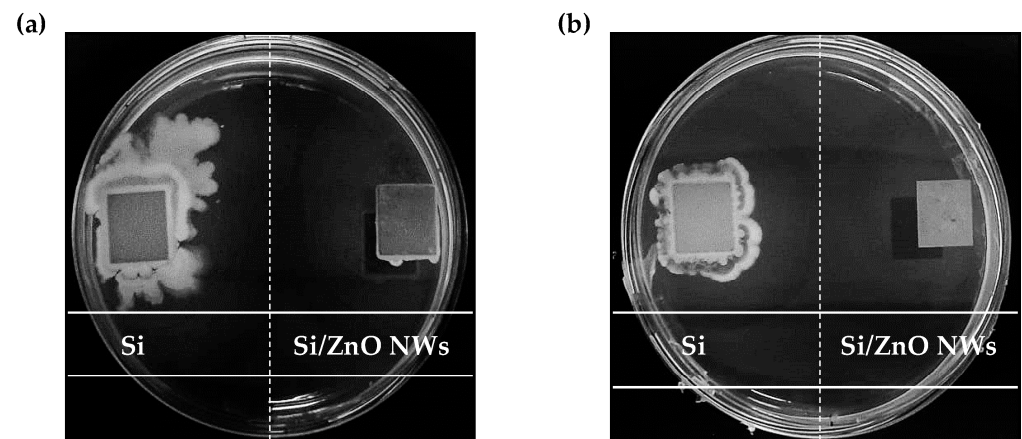


Figure 7. Photo images attesting for the antimicrobial activity against *P. putida* of the prepared ZnO NWs against bare Si: (a) in the dark and (b) under UV light (10 min; 0.17 W/cm^2) utilizing the printing method.

The antibacterial activity of ZnO NWs should not only be attributed to their shape and photoactivity but also to the presence of released zinc ions. It is important to consider these ions as they play a role in the decomposition of bacterial cells, enhancing the overall antibacterial effect. The effect of zinc ions on the antibacterial activity of ZnO NWs against *P. putida* was investigated in which the release of Zn ions from ZnO NWs was measured in two conditions: a sterile M2 medium (control, labeled S1) and a *P. putida* culture M2' (4.1×10^7 CFU/mL, labeled S2). The concentrations of released Zn²⁺ were measured over time and are reproduced in Figure 8a. The results show a similar trend in both cases: an immediate increase in released zinc ions between 0 and 6 h, followed by a slight decrease between 6 and 8 h, and a further decrease from 8 to 24 h. The zinc concentration finally stabilizes around 0.43 mg/mL. However, a higher concentration of released Zn²⁺ ions was observed in the bacterial culture (S2) as compared to the control (S1) between 0 and 6 h (1.44 mg/mL in S2 compared to 1.16 mg/mL in S1). The presence of bacteria, their metabolic activity, and their interaction with the ZnO NWs probably contribute to this difference in zinc ion release. The subsequent decrease from 8 to 24 h and the stabilization at 0.43 mg/mL may indicate a balance between the dissolution of ZnO NWs and the precipitation or adsorption of Zn²⁺. This stability was maintained up to 96 h.

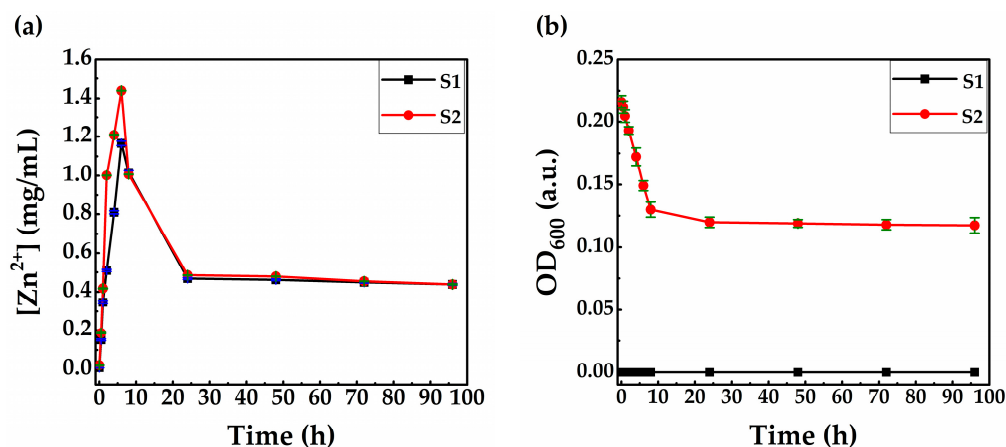


Figure 8. (a) Zn²⁺ released from ZnO NWs into a sterile medium as a control (S1) and the *P. putida* medium (S2) over time. (b) Growth curves through optical density (OD_{600 nm}) measurements.

In parallel to measuring Zn²⁺ release, the OD₆₀₀ was monitored over time in M2 and M2' (Figure 8b) as an indicator of bacterial cell concentration. The OD₆₀₀ values in M2 were below the detection limits of the spectrometer, which is expected since M2 was used as an abiotic control. In M2', we observed a decay effect in the optical density (OD₆₀₀) values over time, from 0.216 ± 0.012 at 0 h to 0.117 ± 0.009 at 96 h. This decline was particularly sharp within the first 6 h, which also corresponds to the hours of the intense release of Zn²⁺ in solution. This suggests that Zn²⁺ could be responsible for the death of bacteria. The stabilization of OD₆₀₀ after 24 h correlates with the Zn²⁺ plateau concentration. This may indicate that a concentration of 0.4 mg/mL is not sufficient to induce bacterial death, and ROS is essential to perform a total disinfection.

4. Discussion

The antibacterial activity of ZnO nanostructures has sparked significant interest due to their multifunctional properties and potential applicability in various domains. Understanding the mechanisms underlying their antibacterial efficacy is essential for exploiting their potential in combating bacterial infections. This discussion section aims to delve into the intricate mechanisms of ZnO nanostructures' antibacterial activity, drawing from the diverse literature and our own research findings.

To begin, it is crucial to comprehend the structure and composition of bacterial cells, as well as the fundamental principles of antibacterial activity. Bacteria are typically composed of a cell membrane, cell wall, and cytoplasm. The cell wall, which consists primarily of a

peptidoglycan layer of amino acids and sugars, is located outside the cell membrane. It plays a crucial role in maintaining the cell shape and osmotic pressure. Gram-negative bacteria, such as *P. Putida*, have two cell membranes, an outer membrane and a plasma membrane, with a thin layer of peptidoglycan about 7–8 nm thick between them [73]. The cytoplasm, a gel-like substance that fills the cell, contains various cellular components except for the nucleus. It facilitates growth, metabolism, and replication and consists of proteins, carbohydrates, nucleic acids, salts, ions, and water (about 80% of the composition) [74]. These components contribute to the electrical conductivity of the cell structure, making the overall charge of bacterial cell walls negative [48].

According to *The American Heritage Medical Dictionary 2007*, antibacterial activity refers to the action of destroying or inhibiting bacterial growth [75]. It is also influenced by the amount of surface area in contact with microorganisms [76]. Antibacterial agents, on the other hand, are selective drugs that specifically target and damage or inhibit bacterial growth without harming the host organism. They serve as chemotherapeutic agents to treat or prevent bacterial infections, as described in the *Saunders Comprehensive Veterinary Dictionary 2007*. An antibacterial agent can be classified as bactericidal if it kills bacteria or bacteriostatic if it inhibits their growth [48].

ZnO nanostructures have attracted considerable research interest due to their multifunctional properties, particularly their antibacterial activity. One of the main advantages of ZnO nanostructures is their potential biocompatibility and low toxicity compared to other metal oxides. Various methods have been employed to study and evaluate their antibacterial activity [77]. Some researchers have evaluated antibacterial activity by measuring bacterial growth through culture turbidity and viable cell percentage through colony counts [78]. Others, such as Yamamoto [79], have improved the antibacterial activity of ZnO nanostructures by manipulating certain parameters. When measuring the variation in electrical conductivity alongside bacterial growth, Yamamoto found that the antibacterial efficacy of ZnO increased as the particle size decreased and the powder concentration increased.

Typically, antibacterial testing is performed in aqueous media or cell culture media. However, ZnO is nearly insoluble in water and tends to agglomerate during synthesis due to the high polarity of water, causing deposition issues such as aggregation, reprecipitation, settling, or nondissolution. To overcome this challenge, researchers have used certain additives that do not significantly affect antibacterial activity. This has motivated many researchers to develop selective nanostructured ZnO specifically designed for antibacterial tests [80–82]. Another area of current research focus is the impact of ZnO shapes, as each morphology contributes to a specific mechanism of action [54,83,84]. Along with morphology, other factors influencing antibacterial activity include UV illumination, ZnO particle size, concentration, surface modification by annealing, surface defects, minimum inhibitory concentration (MIC), and minimum bactericidal concentration (MBC) [85–87].

As mentioned earlier in the introduction, several mechanisms for the antibacterial activity of ZnO nanostructures have been proposed in the literature. These mechanisms include the direct contact of ZnO with bacterial cell walls, leading to the destruction of cell integrity [49,87,88], release of antimicrobial ions, primarily Zn^{2+} [89,90], and the formation of reactive oxygen species (ROS) [91–93]. The mechanism of the antibacterial activity of ZnO nanostructures has been the subject of several discussions. However, it remains incompletely understood and controversial, with certain aspects of the antibacterial activity necessitating in-depth explanations. For example, several studies indicated ROS formation as the main mechanism responsible for ZnO antibacterial activity [91–93]. Raghupathi et al. [78] showed that enhanced ZnO antibacterial activity was due to the increased ROS production from ZnO under UV exposure. Also, Padmavathy et al. [82] proposed an association between photon reaction and antibacterial activity in a series of reactions resulting in the production of hydrogen peroxide (H_2O_2) molecules which penetrate the cell membrane, causing fatal damage. When ZnO is irradiated with UV light having a photon energy larger than (or equal to) the band gap of ZnO, electrons (e^-) of the VB can pass to the CB leaving an equal number of holes (h^+) in the VB, as shown in Equation (9).

The generated holes may react with surface hydroxyls or water ($\text{OH}^-/\text{H}_2\text{O}$) to produce hydroxyl radicals ($\bullet\text{OH}$) on the ZnO surface, which serve as principal oxidants in the photocatalytic system (Equation (10)), while the CB electrons could react with molecular O_2 adsorbed on the ZnO surface to generate superoxide radicals ($\text{O}_2^{\bullet-}$) (Equation (11)). The $\bullet\text{OH}$ free radical plays an important role in damaging the cell wall and cell membrane when it encounters the bacteria cell wall, $\text{O}_2^{\bullet-}$, causing substantial antibacterial activity.



Sawai et al. [92] also attributed the disruption of the cell membrane to the peroxidation of unsaturated phospholipids as a result of photocatalytic-prompted H_2O_2 . However, the role of ROS in antimicrobial actions has become an issue of argument among researchers in this field [78]. The creation of ROS seems to be contradictory since a number of studies have revealed this mechanism under light exposure, as mentioned earlier, while alternative studies have reported the antibacterial activity of ZnO even in the dark [88,94]. The creation of ROS in the dark was observed by Hirota et al. [94] by testing ZnO NPs toward *E. coli*. They found that the activity can occur under darkness, producing superoxide species. Therefore, further studies are required to explain these findings deeply.

Another proposed antibacterial mechanism for ZnO is the release of Zn^{2+} in media containing ZnO and bacteria [89,90]. Pasquet et al. [95] summarized that the Zn^{2+} release mechanism is affected by two main parameters: (i) the physicochemical properties of the particles (including porosity, concentration, particle size, and morphology) and (ii) the chemistry of the media (the pH, UV illumination, exposure time, and existence of other elements). The released Zn^{2+} can significantly inhibit active transport and disrupt amino acid metabolism and enzyme systems, leading to the death of bacterial cells. However, the exact mechanisms by which ZnO exerts its antibacterial activity are not yet fully understood.

After an extensive review of the literature on the antibacterial properties of ZnO, it is evident that numerous studies have concentrated on the antibacterial effects of ZnO NPs. In our research, we successfully demonstrated the antibacterial efficacy of ZnO NWs without the requirement for extra additives, which differs from previous studies. Our study highlighted that the highly textured ZnO NW “forest”, showcased in Figure 4a, has the capability to create a surface displaying nearly 100% antibacterial activity against *P. putida* bacteria. This exceptional antibacterial behavior is attributed to the distinctive morphology of the prepared ZnO NWs, resembling that observed on the wings of *P. claripennis*, which have also exhibited notable antibacterial properties according to references [20–22], as outlined in the introduction section. The distinct shape of our ZnO NWs appeared to be critical in physically impeding the proliferation of *P. putida*, even without the presence of UV light, as evidenced in Figure 7a,b, implying their capacity to interact with and disrupt bacterial cell walls, thus inhibiting bacterial growth and reproduction. Furthermore, the antibacterial efficacy of our ZnO NWs was found to be intensified by UV light, which potentially triggers the generation of ROS, ultimately leading to the complete eradication of bacteria, as demonstrated in Figure 7b. Our findings are consistent with prior research, suggesting that the enhanced antibacterial response of ZnO can be attributed to its morphology [54,83,84] and the increased production of ROS under UV light [78,87–89]. Another study also confirmed the antibacterial effect of *P. claripennis*-inspired nanowire structures formed through the hydrothermal synthesis of ZnO cores and subsequent deposition of SiO_2 shells [54]. This study showcased that the nanowires’ surface utilized a mechanical fracture mechanism to achieve 99% antibacterial efficiency against *E. coli*, further support-

ing our hypothesis that the distinct shape characteristics of our ZnO NWs play a vital role in their antibacterial activity.

Adding to these findings, the measurement of Zn^{2+} concentration in the dissolution experiment of ZnO NWs (Figure 8a) has provided valuable insights into the underlying mechanisms. We showed that Zn^{2+} can be released significantly from the ZnO sample in the presence of the bacterial medium, and the presence of bacteria further enhances this release compared to the abiotic control experiment. Importantly, the correlation between the Zn^{2+} concentration values (strong increase the first 6 h, then decrease and concentration plateau around 0.4 mg/L) and the OD_{600} data (exponential decay; Figure 8b) strengthens the hypothesis that the release of Zn^{2+} is a crucial factor in inhibiting bacterial growth. Furthermore, our findings suggested the existence of a threshold concentration of Zn^{2+} which determines its effectiveness in killing bacteria.

Nevertheless, additional research is required to fully elucidate the mechanisms driving the antibacterial activity of ZnO nanostructures and validate these preliminary findings.

5. Conclusions

To summarize, we successfully synthesized homogeneous and well-ordered ZnO NWs via an environmentally and cost-efficient hydrothermal bottom-up technique. The aim was to assess their photocatalytic and antibacterial properties and to understand the correlation between these two capabilities.

Initially, morphological and optical examinations were conducted on the synthesized ZnO NWs. SEM analysis showed that the nanowires were uniformly vertically aligned, with a mean diameter and length of about 45 nm and 1.5 μm , respectively, and a density of approximately 115 per μm^2 . UV-vis spectroscopy allowed us to deduce the optical band gap of the ZnO NWs, which was found to be 3.22 ± 0.01 eV.

The photocatalytic efficacy of the ZnO NWs in purifying water was then put to the test, using MB as a model pollutant. The prepared ZnO NWs achieved a total photodegradation of MB under UV light (365 nm, 35 mW/cm^2), starting with an initial concentration of 10 μM and completing within 2 h.

Significantly, our research highlighted the potent antibacterial properties of ZnO NWs. They demonstrated an inhibitory effect, with and without UV light, against *P. putida*, a Gram-negative bacterium. This antibacterial action was attributed to three distinguished mechanisms: the direct contact of ZnO NWs with bacterial cell membranes, the release of Zn^{2+} , and the generation of ROS. In dark conditions, the physical attributes of ZnO NWs along with the chemical action of released ions were instrumental for the observed antibacterial efficacy. With a UV light exposure of 10 min at 0.17 W/cm^2 , coupled with the other two mechanisms, the ZnO NWs exhibited an antibacterial activity close to 100%, thanks to the presence of ROS generated by a photocatalytic process.

These findings underscore the vast potential of ZnO NWs as a versatile material with noteworthy photocatalytic and antibacterial activities. This paves the way for a range of applications, particularly in fields demanding efficient antibacterial properties.

Despite our results being substantial, detailed quantitative studies are essential for a full comprehension of the exact mechanisms involved. Hence, future research will delve into the explicit antibacterial activities of ZnO NWs against both Gram-negative and Gram-positive bacteria, providing a broader evaluation of their effectiveness.

Author Contributions: Conceptualization, S.A.Z. and Y.L.-W.; methodology, S.A.Z., A.P., M.L.P. and Y.L.-W.; validation, S.A.Z., A.P., S.R., S.B. and Y.L.-W.; formal analysis, S.A.Z., A.P. and Y.L.-W.; investigation, S.A.Z., A.P. and S.B.; writing—original draft preparation, S.A.Z.; writing—review and editing, S.A.Z., A.P. and Y.L.-W.; visualization, S.A.Z., A.P., S.B., M.L.P., S.R., H.R., N.H. and Y.L.-W.; supervision, Y.L.-W., N.H., S.R. and H.R.; project administration, Y.L.-W.; funding acquisition, N.H., M.L.P. and Y.L.-W. All authors have read and agreed to the published version of the manuscript.

Funding: This work has received support under the program “Investissement d’Avenir” launched by the French Government and implemented by ANR, with the reference ANR-16-IDEX-0003.

Institutional Review Board Statement: Not applicable.

Informed Consent Statement: Not applicable.

Data Availability Statement: Data are contained within the article.

Conflicts of Interest: The authors declare no conflicts of interest.

References

1. Boucher, H.W.; Talbot, G.H.; Bradley, J.S.; Edwards, J.E.; Gilbert, D.; Rice, L.B.; Scheld, M.; Spellberg, B.; Bartlett, J. Bad Bugs, No Drugs: No ESCAPE! An Update from the Infectious Diseases Society of America. *Clin. Infect. Dis.* **2009**, *48*, 1–12. [[CrossRef](#)] [[PubMed](#)]
2. Levy, S.B.; Marshall, B. Antibacterial Resistance Worldwide: Causes, Challenges and Responses. *Nat. Med.* **2004**, *10*, S122–S129. [[CrossRef](#)] [[PubMed](#)]
3. Spellberg, B.; Guidos, R.; Gilbert, D.; Bradley, J.; Boucher, H.W.; Scheld, W.M.; Bartlett, J.G.; Edwards, J., Jr.; Infectious Diseases Society of America. The Epidemic of Antibiotic-Resistant Infections: A Call to Action for the Medical Community from the Infectious Diseases Society of America. *Clin. Infect. Dis.* **2008**, *46*, 155–164. [[CrossRef](#)] [[PubMed](#)]
4. Rodvold, K.A.; McConeghy, K.W. Methicillin-Resistant Staphylococcus Aureus Therapy: Past, Present, and Future. *Clin. Infect. Dis. Off. Publ. Infect. Dis. Soc. Am.* **2014**, *58* (Suppl. S1), S20–S27. [[CrossRef](#)] [[PubMed](#)]
5. O'Neill, J. *Tackling Drug-Resistant Infections Globally: Final Report and Recommendations*; Government of the United Kingdom: London, UK, 2016.
6. Knetsch, M.L.W.; Koole, L.H. New Strategies in the Development of Antimicrobial Coatings: The Example of Increasing Usage of Silver and Silver Nanoparticles. *Polymers* **2011**, *3*, 340–366. [[CrossRef](#)]
7. Ivanova, E.P.; Hasan, J.; Truong, V.K.; Wang, J.Y.; Raveggi, M.; Fluke, C.; Crawford, R.J. The Influence of Nanoscopically Thin Silver Films on Bacterial Viability and Attachment. *Appl. Microbiol. Biotechnol.* **2011**, *91*, 1149–1157. [[CrossRef](#)] [[PubMed](#)]
8. Ivanova, E.P.; Truong, V.K.; Webb, H.K.; Baulin, V.A.; Wang, J.Y.; Mohammedi, N.; Wang, F.; Fluke, C.; Crawford, R.J. Differential Attraction and Repulsion of Staphylococcus Aureus and Pseudomonas Aeruginosa on Molecularly Smooth Titanium Films. *Sci. Rep.* **2011**, *1*, 165. [[CrossRef](#)] [[PubMed](#)]
9. Menéndez Miranda, M.; Liu, W.; Godinez-Leon, J.A.; Amanova, A.; Houel-Renault, L.; Lampre, I.; Remita, H.; Gref, R. Colloidal Silver Nanoparticles Obtained via Radiolysis: Synthesis Optimization and Antibacterial Properties. *Pharmaceutics* **2023**, *15*, 1787. [[CrossRef](#)] [[PubMed](#)]
10. Källicke, T.; Schierholz, J.; Schlegel, U.; Frangen, T.M.; Köller, M.; Printzen, G.; Seybold, D.; Klöckner, S.; Muhr, G.; Arens, S. Effect on Infection Resistance of a Local Antiseptic and Antibiotic Coating on Osteosynthesis Implants: An in Vitro and in Vivo Study. *J. Orthop. Res. Off. Publ. Orthop. Res. Soc.* **2006**, *24*, 1622–1640. [[CrossRef](#)] [[PubMed](#)]
11. Banerjee, I.; Pangule, R.C.; Kane, R.S. Antifouling Coatings: Recent Developments in the Design of Surfaces That Prevent Fouling by Proteins, Bacteria, and Marine Organisms. *Adv. Mater.* **2011**, *23*, 690–718. [[CrossRef](#)] [[PubMed](#)]
12. Nederberg, F.; Zhang, Y.; Tan, J.P.K.; Xu, K.; Wang, H.; Yang, C.; Gao, S.; Guo, X.D.; Fukushima, K.; Li, L.; et al. Biodegradable Nanostructures with Selective Lysis of Microbial Membranes. *Nat. Chem.* **2011**, *3*, 409–414. [[CrossRef](#)] [[PubMed](#)]
13. Elbourne, A.; Chapman, J.; Gelmi, A.; Cozzolino, D.; Crawford, R.J.; Truong, V.K. Bacterial-Nanostructure Interactions: The Role of Cell Elasticity and Adhesion Forces. *J. Colloid Interface Sci.* **2019**, *546*, 192–210. [[CrossRef](#)] [[PubMed](#)]
14. Elbourne, A.; Truong, V.K.; Cheeseman, S.; Rajapaksha, P.; Gangadoo, S.; Chapman, J.; Crawford, R. The Use of Nanomaterials for the Mitigation of Pathogenic Biofilm Formation. *Methods Microbiol.* **2019**, *46*, 61–92. [[CrossRef](#)]
15. Bridier, A.; Briandet, R.; Thomas, V.; Dubois-Brissonnet, F. Resistance of Bacterial Biofilms to Disinfectants: A Review. *Biofouling* **2011**, *27*, 1017–1032. [[CrossRef](#)]
16. Johnston, H.J.; Hutchison, G.; Christensen, F.M.; Peters, S.; Hankin, S.; Stone, V. A Review of the in Vivo and in Vitro Toxicity of Silver and Gold Particulates: Particle Attributes and Biological Mechanisms Responsible for the Observed Toxicity. *Crit. Rev. Toxicol.* **2010**, *40*, 328–346. [[CrossRef](#)] [[PubMed](#)]
17. Stigter, M.; Bezemer, J.; de Groot, K.; Layrolle, P. Incorporation of Different Antibiotics into Carbonated Hydroxyapatite Coatings on Titanium Implants, Release and Antibiotic Efficacy. *J. Control. Release Off. J. Control. Release Soc.* **2004**, *99*, 127–137. [[CrossRef](#)] [[PubMed](#)]
18. Jang, Y.; Choi, W.T.; Johnson, C.T.; García, A.J.; Singh, P.M.; Breedveld, V.; Hess, D.W.; Champion, J.A. Inhibition of Bacterial Adhesion on Nanotextured Stainless Steel 316L by Electrochemical Etching. *ACS Biomater. Sci. Eng.* **2018**, *4*, 90–97. [[CrossRef](#)] [[PubMed](#)]
19. Onaizi, S.A.; Leong, S.S.J. Tethering Antimicrobial Peptides: Current Status and Potential Challenges. *Biotechnol. Adv.* **2011**, *29*, 67–74. [[CrossRef](#)] [[PubMed](#)]
20. Pogodin, S.; Hasan, J.; Baulin, V.A.; Webb, H.K.; Truong, V.K.; Phong Nguyen, T.H.; Boshkovikj, V.; Fluke, C.J.; Watson, G.S.; Watson, J.A.; et al. Biophysical Model of Bacterial Cell Interactions with Nanopatterned Cicada Wing Surfaces. *Biophys. J.* **2013**, *104*, 835–840. [[CrossRef](#)] [[PubMed](#)]

21. Ivanova, E.P.; Hasan, J.; Webb, H.K.; Truong, V.K.; Watson, G.S.; Watson, J.A.; Baulin, V.A.; Pogodin, S.; Wang, J.Y.; Tobin, M.J.; et al. Natural Bactericidal Surfaces: Mechanical Rupture of *Pseudomonas Aeruginosa* Cells by Cicada Wings. *Small* **2012**, *8*, 2489–2494. [[CrossRef](#)] [[PubMed](#)]
22. Tripathy, A.; Sen, P.; Su, B.; Briscoe, W.H. Natural and Bioinspired Nanostructured Bactericidal Surfaces. *Adv. Colloid Interface Sci.* **2017**, *248*, 85–104. [[CrossRef](#)] [[PubMed](#)]
23. Elbourne, A.; Crawford, R.J.; Ivanova, E.P. Nano-Structured Antimicrobial Surfaces: From Nature to Synthetic Analogues. *J. Colloid Interface Sci.* **2017**, *508*, 603–616. [[CrossRef](#)] [[PubMed](#)]
24. Luong-Van, E.; Rodriguez, I.; Low, H.Y.; Elmouelhi, N.; Lowenhaupt, B.; Natarajan, S.; Lim, C.T.; Prajapati, R.; Vyakarnam, M.; Cooper, K. Review: Micro- and Nanostructured Surface Engineering for Biomedical Applications. *J. Mater. Res.* **2013**, *28*, 165–174. [[CrossRef](#)]
25. Linklater, D.P.; Juodkazis, S.; Ivanova, E.P. Nanofabrication of Mechano-Bactericidal Surfaces. *Nanoscale* **2017**, *9*, 16564–16585. [[CrossRef](#)] [[PubMed](#)]
26. Li, X. Bactericidal Mechanism of Nanopatterned Surfaces. *Phys. Chem. Chem. Phys.* **2016**, *18*, 1311–1316. [[CrossRef](#)] [[PubMed](#)]
27. Nguyen, K.N.; Basset, P.; Marty, F.; Leprince-Wang, Y.; Bourouina, T. On the Optical and Morphological Properties of Microstructured Black Silicon Obtained by Cryogenic-Enhanced Plasma Reactive Ion Etching. *J. Appl. Phys.* **2013**, *113*, 194903. [[CrossRef](#)]
28. Ivanova, E.P.; Hasan, J.; Webb, H.K.; Gervinskas, G.; Juodkazis, S.; Truong, V.K.; Wu, A.H.F.; Lamb, R.N.; Baulin, V.A.; Watson, G.S.; et al. Bactericidal Activity of Black Silicon. *Nat. Commun.* **2013**, *4*, 2838. [[CrossRef](#)]
29. Arias, A.C.; MacKenzie, J.D.; McCulloch, I.; Rivnay, J.; Salleo, A. Materials and Applications for Large Area Electronics: Solution-Based Approaches. *Chem. Rev.* **2010**, *110*, 3–24. [[CrossRef](#)] [[PubMed](#)]
30. Diodati, S.; Dolcet, P.; Casarin, M.; Gross, S. Pursuing the Crystallization of Mono- and Polymetallic Nanosized Crystalline Inorganic Compounds by Low-Temperature Wet-Chemistry and Colloidal Routes. *Chem. Rev.* **2015**, *115*, 11449–11502. [[CrossRef](#)] [[PubMed](#)]
31. Zhang, J. Silver-Coated Zinc Oxide Nanoantibacterial Synthesis and Antibacterial Activity Characterization. In Proceedings of the ICEOE 2011—2011 International Conference on Electronics and Optoelectronics, Dalian, China, 29–31 July 2011; Volume 3. [[CrossRef](#)]
32. Firouzabadi, F.B.; Noori, M.; Edalatpanah, Y.; Mirhosseini, M. ZnO Nanoparticle Suspensions Containing Citric Acid as Antimicrobial to Control *Listeria Monocytogenes*, *Escherichia Coli*, *Staphylococcus Aureus* and *Bacillus Cereus* in Mango Juice. *Food Control* **2014**, *42*, 310–314. [[CrossRef](#)]
33. Ruffolo, S.A.; La Russa, M.F.; Malagodi, M.; Oliviero Rossi, C.; Palermo, A.M.; Crisci, G.M. ZnO and ZnTiO₃ Nanopowders for Antimicrobial Stone Coating. *Appl. Phys. A* **2010**, *100*, 829–834. [[CrossRef](#)]
34. Butcher, P.N.; March, N.H.; Tosi, M.P. (Eds.) *Crystalline Semiconducting Materials and Devices*, 1st ed.; Springer: New York, NY, USA, 1986; ISBN 9781475799026.
35. Petkov, P.; Tsiulyanu, D.; Popov, C.; Kulisch, W. *Nanoscience Advances in CBRN Agent Detection, Information and Energy Security: An Introduction*; Springer: Dordrecht, The Netherlands, 2015; pp. 3–13.
36. Gomez, J.L.; Tigli, O. Zinc Oxide Nanostructures: From Growth to Application. *J. Mater. Sci.* **2013**, *48*, 612–624. [[CrossRef](#)]
37. Wang, Z.L. Zinc Oxide Nanostructures: Growth, Properties and Applications. *J. Phys. Condens. Matter* **2004**, *16*, R829. [[CrossRef](#)]
38. Schmidt-Mende, L.; MacManus-Driscoll, J.L. ZnO—Nanostructures, Defects, and Devices. *Mater. Today* **2007**, *10*, 40–48. [[CrossRef](#)]
39. Özgür, Ü.; Alivov, Y.I.; Liu, C.; Teke, A.; Reshchikov, M.A.; Doğan, S.; Avrutin, V.; Cho, S.-J.; Morkoç, H. A Comprehensive Review of ZnO Materials and Devices. *J. Appl. Phys.* **2005**, *98*, 41301. [[CrossRef](#)]
40. Le Pivert, M.; Kerivel, O.; Zerelli, B.; Leprince-Wang, Y. ZnO Nanostructures Based Innovative Photocatalytic Road for Air Purification. *J. Clean. Prod.* **2021**, *318*, 128447. [[CrossRef](#)]
41. Le Pivert, M.; Martin, N.; Leprince-Wang, Y. Hydrothermally Grown ZnO Nanostructures for Water Purification via Photocatalysis. *Crystals* **2022**, *12*, 308. [[CrossRef](#)]
42. Petersen, E.W.; Likovich, E.M.; Russell, K.J.; Narayanamurti, V. Growth of ZnO Nanowires Catalyzed by Size-Dependent Melting of Au Nanoparticles. *Nanotechnology* **2009**, *20*, 405603. [[CrossRef](#)] [[PubMed](#)]
43. Lim, S.K.; Hwang, S.H.; Kim, S. Microemulsion Synthesis and Characterization of Aluminum Doped ZnO Nanorods. *Cryst. Res. Technol.* **2010**, *45*, 771–775. [[CrossRef](#)]
44. Protasova, L.N.; Rebrov, E.V.; Choy, K.L.; Pung, S.Y.; Engels, V.; Cabaj, M.; Wheatley, A.E.H.; Schouten, J.C. ZnO Based Nanowires Grown by Chemical Vapour Deposition for Selective Hydrogenation of Acetylene Alcohols. *Catal. Sci. Technol.* **2011**, *1*, 768–777. [[CrossRef](#)]
45. Cheng, H.-M.; Chiu, W.-H.; Lee, C.-H.; Tsai, S.-Y.; Hsieh, W.-F. Formation of Branched ZnO Nanowires from Solvothermal Method and Dye-Sensitized Solar Cells Applications. *J. Phys. Chem. C* **2008**, *112*, 16359–16364. [[CrossRef](#)]
46. Hu, H.; Huang, X.; Deng, C.; Chen, X.; Qian, Y. Hydrothermal Synthesis of ZnO Nanowires and Nanobelts on a Large Scale. *Mater. Chem. Phys.* **2007**, *106*, 58–62. [[CrossRef](#)]
47. Chevalier-César, C.; Capochichi-Gnambodoe, M.; Leprince-Wang, Y. Growth Mechanism Studies of ZnO Nanowire Arrays via Hydrothermal Method. *Appl. Phys. A* **2014**, *115*, 953–960. [[CrossRef](#)]
48. Sirelkhatim, A.; Mahmud, S.; Seeni, A.; Kaus, N.H.M.; Ann, L.C.; Bakhori, S.K.M.; Hasan, H.; Mohamad, D. Review on Zinc Oxide Nanoparticles: Antibacterial Activity and Toxicity Mechanism. *Nano-Micro Lett.* **2015**, *7*, 219–242. [[CrossRef](#)] [[PubMed](#)]

49. Brayner, R.; Ferrari-Iliou, R.; Brivois, N.; Djediat, S.; Benedetti, M.F.; Fiévet, F. Toxicological Impact Studies Based on Escherichia Coli Bacteria in Ultrafine ZnO Nanoparticles Colloidal Medium. *Nano Lett.* **2006**, *6*, 866–870. [CrossRef] [PubMed]
50. Yamamoto, O.; Komatsu, M.; Sawai, J.; Nakagawa, Z.-E. Effect of Lattice Constant of Zinc Oxide on Antibacterial Characteristics. *J. Mater. Sci. Mater. Med.* **2004**, *15*, 847–851. [CrossRef]
51. Lipovsky, A.; Nitzan, Y.; Gedanken, A.; Lubart, R. Antifungal Activity of ZnO Nanoparticles—The Role of ROS Mediated Cell Injury. *Nanotechnology* **2011**, *22*, 105101. [CrossRef] [PubMed]
52. Dwivedi, S.; Wahab, R.; Khan, F.; Mishra, Y.K.; Musarrat, J.; Al-Khedhairi, A.A. Reactive Oxygen Species Mediated Bacterial Biofilm Inhibition via Zinc Oxide Nanoparticles and Their Statistical Determination. *PLoS ONE* **2014**, *9*, e111289. [CrossRef] [PubMed]
53. Lakshmi Prasanna, V.; Vijayaraghavan, R. Insight into the Mechanism of Antibacterial Activity of ZnO: Surface Defects Mediated Reactive Oxygen Species Even in the Dark. *Langmuir* **2015**, *31*, 9155–9162. [CrossRef] [PubMed]
54. Shimada, T.; Yasui, T.; Yonese, A.; Yanagida, T.; Kaji, N.; Kanai, M.; Nagashima, K.; Kawai, T.; Baba, Y. Mechanical Rupture-Based Antibacterial and Cell-Compatible ZnO/SiO₂ Nanowire Structures Formed by Bottom-Up Approaches. *Micromachines* **2020**, *11*, 610. [CrossRef] [PubMed]
55. Martin, N.; Leprince-Wang, Y. HPLC-MS and UV-Visible Coupled Analysis of Methylene Blue Photodegradation by Hydrothermally Grown ZnO Nanowires. *Phys. Status Solidi* **2021**, *218*, 2100532. [CrossRef]
56. Habba, Y.G.; Capochichi-Gnambodoe, M.; Serairi, L.; Leprince-Wang, Y. Enhanced Photocatalytic Activity of ZnO Nanostructure for Water Purification. *Phys. Status Solidi* **2016**, *253*, 1480–1484. [CrossRef]
57. Valbi, V.; Perez, A.; Verney-Carron, A.; Rossano, S. Impact of a Mn-Oxidizing Bacterial Strain on the Dissolution and Browning of a Mn-Bearing Potash-Lime Silicate Glass. *Npj Mater. Degrad.* **2023**, *7*, 20. [CrossRef]
58. Postgate, J.R. Chapter XVIII Viable Counts and Viability. In *Methods in Microbiology*; Norris, J.R., Ribbons, D.W., Eds.; Academic Press: Cambridge, MA, USA, 1969; Volume 1, pp. 611–628. ISBN 0580-9517.
59. Le Pivert, M.; Suo, H.; Tang, G.; Qiao, H.; Zhao, Z.; Martin, N.; Liu, C.; Leprince-Wang, Y. Improving Natural Sunlight Photocatalytic Efficiency of ZnO Nanowires Decorated by Iron Oxide Cocatalyst via a Simple Drop Method. *Mater. Chem. Phys.* **2022**, *275*, 125304. [CrossRef]
60. Patil, A.; Dighavkar, C.; Sonawane, S.; Patil, S.; Borse, R. Effect of Firing Temperature on Electrical and Structural Characteristics of Screen Printed ZnO Thick Films. *OAM-RC* **2009**, *3*, 879–883.
61. Pankove, J.I. *Optical Processes in Semiconductors*; Prentice-Hall: Englewood Cliffs, NJ, USA, 1979; ISBN 9780136380238, 0136380239.
62. Tauc, J. Optical Properties and Electronic Structure of Amorphous Ge and Si. *Mater. Res. Bull.* **1968**, *3*, 37–46. [CrossRef]
63. Çolak, H.; Karaköse, E.; Kartopu, G. Effect of Consumption of the Sol-Gel Deposited ZnO Seed Layer on the Growth and Properties of High Quality ZnO Nanorods. *J. Mater. Sci. Mater. Electron.* **2018**, *29*, 11964–11971. [CrossRef]
64. Qi, K.; Xing, X.; Zada, A.; Li, M.; Wang, Q.; Liu, S.; Lin, H.; Wang, G. Transition Metal Doped ZnO Nanoparticles with Enhanced Photocatalytic and Antibacterial Performances: Experimental and DFT Studies. *Ceram. Int.* **2020**, *46*, 1494–1502. [CrossRef]
65. Chitra, M.; Mangamma, G.; Uthayarani, K.; Neelakandeswari, N.; Girija, E.K. Band Gap Engineering in ZnO Based Nanocomposites. *Phys. E Low-Dimens. Syst. Nanostructures* **2020**, *119*, 113969. [CrossRef]
66. Rai, R.C.; Guminiak, M.; Wilser, S.; Cai, B.; Nakarmi, M.L. Elevated Temperature Dependence of Energy Band Gap of ZnO Thin Films Grown by E-Beam Deposition. *J. Appl. Phys.* **2012**, *111*, 73511. [CrossRef]
67. Wang, Y.; Yang, J.; Jia, H.; Yu, M.; Jin, H. Self-Assembled Urchin-like ZnO Nanostructures Fabricated by Electrodeposition-Hydrothermal Method. *J. Alloys Compd.* **2016**, *665*, 62–68. [CrossRef]
68. Mcpeak, K.; Le, T.; Britton, N.; Nickolov, Z.; Elabd, Y.; Baxter, J. Chemical Bath Deposition of ZnO Nanowires at Near-Neutral PH Conditions without Hexamethylenetetramine (HMTA): Understanding the Role of HMTA in ZnO Nanowire Growth. *Langmuir* **2011**, *27*, 3672–3677. [CrossRef] [PubMed]
69. Greene, L.E.; Yuhas, B.D.; Law, M.; Zitoun, D.; Yang, P. Solution-Grown Zinc Oxide Nanowires. *Inorg. Chem.* **2006**, *45*, 7535–7543. [CrossRef]
70. Xie, W.; Li, Y.; Sun, W.; Huang, J.C.; Xie, H.; Zhao, X. Surface Modification of ZnO with Ag Improves Its Photocatalytic Efficiency and Photostability. *J. Photochem. Photobiol. A-Chem.* **2010**, *216*, 149–155. [CrossRef]
71. Yang, L.-Y.; Dong, S.-Y.; Sun, J.-H.; Feng, J.-L.; Wu, Q.-H.; Sun, S.-P. Microwave-Assisted Preparation, Characterization and Photocatalytic Properties of a Dumbbell-Shaped ZnO Photocatalyst. *J. Hazard. Mater.* **2010**, *179*, 438–443. [CrossRef] [PubMed]
72. Yang, C.; Li, Q.; Tang, L.; Xin, K.; Bai, A.; Yu, Y. Synthesis, Photocatalytic Activity, and Photogenerated Hydroxyl Radicals of Monodisperse Colloidal ZnO Nanospheres. *Appl. Surf. Sci.* **2015**, *357*, 1928–1938. [CrossRef]
73. Fu, G.; Vary, P.S.; Lin, C.-T. Anatase TiO₂ Nanocomposites for Antimicrobial Coatings. *J. Phys. Chem. B* **2005**, *109*, 8889–8898. [CrossRef]
74. Edwards, J.V.A.; Edwards, K.J. Bacteria Cell. Available online: <http://www.alken-murray.com/BioInfo1-05.html> (accessed on 9 July 2010).
75. Di, A.H.; Houghton Mifflin Company (Eds.) *The American Heritage Medical Dictionary*; Houghton Mifflin Company: Boston, MA, USA, 2007; ISBN 9780618824359.
76. Wahab, R.; Kim, Y.-S.; Mishra, A.; Yun, S.-I.; Shin, H.-S. Formation of ZnO Micro-Flowers Prepared via Solution Process and Their Antibacterial Activity. *Nanoscale Res. Lett.* **2010**, *5*, 1675–1681. [CrossRef]

77. Premanathan, M.; Karthikeyan, K.; Jeyasubramanian, K.; Manivannan, G. Selective Toxicity of ZnO Nanoparticles toward Gram-Positive Bacteria and Cancer Cells by Apoptosis through Lipid Peroxidation. *Nanomedicine* **2011**, *7*, 184–192. [[CrossRef](#)]
78. Raghupathi, K.R.; Koodali, R.T.; Manna, A.C. Size-Dependent Bacterial Growth Inhibition and Mechanism of Antibacterial Activity of Zinc Oxide Nanoparticles. *Langmuir* **2011**, *27*, 4020–4028. [[CrossRef](#)]
79. Yamamoto, O. Influence of Particle Size on the Antibacterial Activity of Zinc Oxide. *Int. J. Inorg. Mater.* **2001**, *3*, 643–646. [[CrossRef](#)]
80. Wahab, R.; Mishra, A.; Yun, S.-I.; Kim, Y.-S.; Shin, H.-S. Antibacterial Activity of ZnO Nanoparticles Prepared via Non-Hydrolytic Solution Route. *Appl. Microbiol. Biotechnol.* **2010**, *87*, 1917–1925. [[CrossRef](#)] [[PubMed](#)]
81. Stanković, A.; Dimitrijević, S.; Uskoković, D. Influence of Size Scale and Morphology on Antibacterial Properties of ZnO Powders Hydrothermally Synthesized Using Different Surface Stabilizing Agents. *Colloids Surf. B. Biointerfaces* **2013**, *102*, 21–28. [[CrossRef](#)] [[PubMed](#)]
82. Padmavathy, N.; Vijayaraghavan, R. Enhanced Bioactivity of ZnO Nanoparticles—an Antimicrobial Study. *Sci. Technol. Adv. Mater.* **2008**, *9*, 35004. [[CrossRef](#)] [[PubMed](#)]
83. Talebian, N.; Amininezhad, S.M.; Doudi, M. Controllable Synthesis of ZnO Nanoparticles and Their Morphology-Dependent Antibacterial and Optical Properties. *J. Photochem. Photobiol. B Biol.* **2013**, *120*, 66–73. [[CrossRef](#)] [[PubMed](#)]
84. Ma, J.; Liu, J.; Bao, Y.; Zhu, Z.; Wang, X.; Zhang, J. Synthesis of Large-Scale Uniform Mulberry-like ZnO Particles with Microwave Hydrothermal Method and Its Antibacterial Property. *Ceram. Int.* **2013**, *39*, 2803–2810. [[CrossRef](#)]
85. Ann, L.; Mahmud, S.; Mohd Bakhori, S.; Sirelkhatim, A.; Mohamad, D.; Hasan, H.; Seeni, A.; Rahman, R. Effect of Surface Modification and UVA Photoactivation on Antibacterial Bioactivity of Zinc Oxide Powder. *Appl. Surf. Sci.* **2014**, *292*, 405–412. [[CrossRef](#)]
86. Mamat, M.H.; Khusaimi, Z.; Zahidi, M.M.; Mahmood, M.R. Performance of an Ultraviolet Photoconductive Sensor Using Well-Aligned Aluminium-Doped Zinc-Oxide Nanorod Arrays Annealed in an Air and Oxygen Environment. *Jpn. J. Appl. Phys.* **2011**, *50*, 06GF05. [[CrossRef](#)]
87. Zhang, L.; Jiang, Y.; Ding, Y.; Povey, M.; York, D. Investigation into the Antibacterial Behaviour of Suspensions of ZnO Nanoparticles (ZnO Nanofluids). *J. Nanoparticle Res.* **2007**, *9*, 479–489. [[CrossRef](#)]
88. Adams, L.K.; Lyon, D.Y.; Alvarez, P.J.J. Comparative Eco-Toxicity of Nanoscale TiO₂, SiO₂, and ZnO Water Suspensions. *Water Res.* **2006**, *40*, 3527–3532. [[CrossRef](#)]
89. Kasemets, K.; Ivask, A.; Dubourguier, H.-C.; Kahru, A. Toxicity of Nanoparticles of ZnO, CuO and TiO₂ to Yeast *Saccharomyces Cerevisiae*. *Toxicol. Vitr. Int. J. Publ. Assoc. BIBRA* **2009**, *23*, 1116–1122. [[CrossRef](#)] [[PubMed](#)]
90. Li, M.; Zhu, L.; Lin, D. Toxicity of ZnO Nanoparticles to *Escherichia Coli*: Mechanism and the Influence of Medium Components. *Environ. Sci. Technol.* **2011**, *45*, 1977–1983. [[CrossRef](#)] [[PubMed](#)]
91. Jalal, R.; Goharshadi, E.K.; Abareshi, M.; Moosavi, M.; Yousefi, A.; Nancarrow, P. ZnO Nanofluids: Green Synthesis, Characterization, and Antibacterial Activity. *Mater. Chem. Phys.* **2010**, *121*, 198–201. [[CrossRef](#)]
92. Sawai, J.; Shoji, S.; Igarashi, H.; Hashimoto, A.; Kokugan, T.; Shimizu, M.; Kojima, H. Hydrogen Peroxide as an Antibacterial Factor in Zinc Oxide Powder Slurry. *J. Ferment. Bioeng.* **1998**, *86*, 521–522. [[CrossRef](#)]
93. Zhang, L.; Ding, Y.; Povey, M.; York, D. ZnO Nanofluids—A Potential Antibacterial Agent. *Prog. Nat. Sci.* **2008**, *18*, 939–944. [[CrossRef](#)]
94. Hirota, K.; Sugimoto, M.; Kato, M.; Tsukagoshi, K.; Tanigawa, T.; Sugimoto, H. Preparation of Zinc Oxide Ceramics with a Sustainable Antibacterial Activity under Dark Conditions. *Ceram. Int.* **2010**, *36*, 497–506. [[CrossRef](#)]
95. Pasquet, J.; Chevalier, Y.; Pelletier, J.; Couval, E.; Bouvier, D.; Bolzinger, M.-A. The Contribution of Zinc Ions to the Antimicrobial Activity of Zinc Oxide. *Colloids Surf. A Physicochem. Eng. Asp.* **2014**, *457*, 263–274. [[CrossRef](#)]

Disclaimer/Publisher’s Note: The statements, opinions and data contained in all publications are solely those of the individual author(s) and contributor(s) and not of MDPI and/or the editor(s). MDPI and/or the editor(s) disclaim responsibility for any injury to people or property resulting from any ideas, methods, instructions or products referred to in the content.